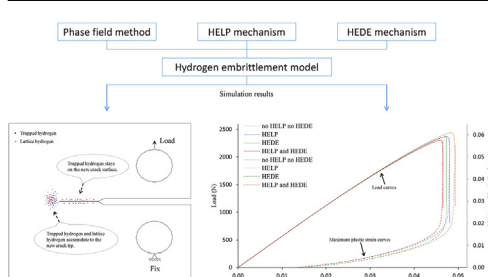# Phase field modeling of hydrogen embrittlement

Chuanshi Huang, Xiaosheng Gao*

Department of Mechanical Engineering, University of Akron, Akron, OH 44325, USA

HIGHLIGHTS

- Hydrogen transport and hydrogen embrittlement mechanisms are combined in a phase field model.
- A hydrogen diffusion equation is derived and a trapping density function is proposed.
- HELP is modeled by a reduction of the yield stress with hydrogen concentration.
- HEDE is modeled by a reduction of the critical energy release rate with hydrogen concentration.
- Simulation results are in qualitative agreement with results of previous investigations.

GRAPHICAL ABSTRACT

ABSTRACT

A numerical framework is developed in this paper to study hydrogen embrittlement. A hydrogen diffusion equation is derived, and a trapping density function is proposed in the framework of the phase field model. Effect of hydrogen enhanced localized plasticity (HELP) and hydrogen enhanced decohesion (HEDE) are modeled by reducing the yield stress and decreasing the critical energy release rate respectively. Simulation results of a compact tension specimen and a double notched tension specimen show that hydrogen accumulates at the crack/notch tip region driven by positive hydrostatic stress as well as more traps produced by plastic deformation in this area. Both HELP and HEDE reduce the load carrying capacity of the specimen, and their effects depend on the model parameters. The proposed model provides a numerical tool that can be used to comprehensively simulate hydrogen embrittlement and predict the ductile to brittle transition of the material due to the presence of hydrogen.

© 2020 Hydrogen Energy Publications LLC. Published by Elsevier Ltd. All rights reserved.

Introduction

Dissolved hydrogen atoms in metals degrade the material's mechanical properties, such as strength and ductility, resulting in material failing at a lower level of load than it can normally bear. This phenomenon is known as hydrogen embrittlement. Johnson first observed the phenomenon of hydrogen embrittlement in 1875 when he immerged a piece of iron in strong hydrochloric or dilute sulphuric acids for a few minutes and found a significant reduction in the ductility of the material [1]. Johnson's experiment has initiated the study of the hydrogen embrittlement of metals [2]. Hydrogen embrittles a variety of materials, and hydrogen-induced cracking often leads to a sudden, catastrophic failure without warning. Hydrogen embrittlement is known as one of the most common failure causes of the high strength steel components in military aircraft. It is also one of the most critical corrosion failures in oil and gas industry as well as in construction.

Hydrogen can be introduced into the material during manufacture or over time through environmental exposure. Hydrogen atoms can diffuse between interstitial lattice sites (NILS) in metals. They can also be trapped by imperfections such as dislocation core. The diffusion process is dominated by the gradients of chemical potential which is characterized by the gradient of the hydrogen concentration in the lattice sites as well as the gradient of the hydrostatic stress. Oriani [3] developed a formulation based on the assumed equilibrium relation that describe the population of the trapped hydrogen and the diffusive hydrogen (lattice hydrogen). Using this theory, Sofronis and McMeeking [4] derived a non-linear hydrogen diffusion equation and studied the coupled transient hydrogen diffusion and plastic straining around a blunting crack tip. They also proposed a function of the equivalent plastic strain for the trap density based on Kumnick and Johnson's experimental observation [5]. Lufrano and Sofronis [6] further modified Sofronis and McMeeking's hydrogen diffusion model by adding the hydrogen induced dilatation to the material constitutive equations.

To interpret hydrogen embrittlement, many mechanisms have been proposed by different researchers, such as hydrogen enhanced decohesion (HEDE) [2,7–9] and hydrogen enhanced localized plasticity (HELP) [10–14]. The HELP effect can reduce the ductility of metals by promoting plastic deformation localization in the ductile fracture process. Beachem [10] conducted torsion tests of the hydrogen charged and hydrogen free steel pipes and observed that hydrogen decreased the local flow stress. Matsui et al.[15] and Moriya et al. [16] systematically studied the effect of hydrogen on mechanical properties of purity iron under different temperatures and hydrogen concentrations. They concluded that trapped hydrogen at the screw dislocation core promote screw dislocations, and on the other hand, hydrogen impedes edge dislocations under a sufficiently low level of temperature. Ferreira et al. [17] observed that the elastic interaction between dislocations was reduced by hydrogen in stainless steel. Robertson [18] performed in-situ TEM deformation experiments on different metals and the results showed persuasive evidence that hydrogen could enhance the mobility of dislocations. Birnbaum and Sofronis [19]

investigated how the dissolved hydrogen influence the interaction of dislocations, and proposed a hydrogen shielding effect to interpret the hydrogen promoted mobility of dislocations. Liang et al. [20] used an axisymmetric unit cell model to investigate the mutual effect between hydrogen and micro-void coalescence under a range of stress triaxialities, and their results suggested that the trapped hydrogen strongly influence the void coalescence process. Huang et al.[16] used a 3D unit cell to investigate how ductile fracture is affected by the HELP mechanism with different stress states imposed on the representative material volume. Luo et al. [22] considered the influence of the of the loading speed on the hydrogen distribution in the material, and studied the HELP effect on ductile fracture under the influence of steady state hydrogen distribution. Yu et al. [23] studied hydrogen-microvoid interactions under the effect of HELP, and investigated the effect of hydrogen on the fracture loci. Depover and Verbeken experimentally observed that the HELP mechanism played an important role in hydrogen embrittlement [24].

Previous studies suggest that hydrogen in metals lowers the surface energy and promote cracking [25–27]. The HEDE mechanism is a result of dissolved hydrogen atoms reducing the strength of atomic bonds of the parent material. Consequently, dissolved hydrogen may cause a transition of the fracture mechanism from ductile to brittle [28]. Troiano [29] introduced the concept that the cohesive strength of the iron lattice is lowered by the dissolved hydrogen. Beachem argued that the presence of sufficiently accumulated lattice hydrogen ahead of the crack tip promotes whatever deformation processes the microstructure allows for and proposed a model to explain various fracture mechanisms [10]. Jiang et al. [30] used the Born-Haber thermodynamic cycle to calculate the fracture energy of hydrogen attacked metals (Fe and Al), and found that fracture energy decreases with the increase of hydrogen concentration. Based on this calculation, Serebrinsky [31] proposed a quadratic relationship between the cohesive strength and the hydrogen concentration. Martínez-Pañeda et al. [32] modeled hydrogen embrittlement by considering the critical energy release rate as a function of hydrogen concentration. Wang et al. [33] conducted atomic simulations to analyze hydrogen-induced decohesion of grain boundary under different hydrogen charging conditions, and observed the occurrence of intergranular fracture when the grain boundary cohesive energy was reduced by 37% due to the presence of hydrogen. They suggested that intergranular fracture is a result of the combination of HEDE and HELP mechanisms.

To comprehensively model hydrogen embrittlement of metals, the numerical method needs to be able to simulate brittle fracture, ductile fracture and the fracture mechanism transition between ductile and brittle. Many numerical models according to different fracture criteria are proposed to simulate the fracture processes of different materials. Among them, the phase field model is not only flexible to implement but also has the ability to simulate complex fracture process, such as crack merging and branching. The phase field model is developed from the Griffith's theory [34], but it does not need a pre-defined crack or a fracture path [35]. The feasibility of this method was demonstrated by Bourdin et al. [36,37]. Miehe et al. [38,39] proposed an algorithm which splits the crack

phase field and the displacement field and applied the phase model to predict brittle fracture, and Miehe et al. [40] further developed their model by including the plastic contribution to predict ductile fracture. Ambati et al. [41,42] introduced the plastic strain state into the degradation function to delay crack initiation, and compared the numerical results with experimental observations. Borden et al. [43] introduced a cubic degradation function and applied it to the yield surface during the fracture process. They also considered the effect of the stress triaxiality on the crack driving force. Huang and Gao [44] modified the model of Miehe et al. [40] by proposing a new approach for material degradation and incorporating a plastic adjustment factor into the crack driving force function. Numerical examples show that this model is capable of simulating the fracture mechanism transition between ductile and brittle.

This study incorporates hydrogen transport in metals and the resulting HELP and HEDE mechanisms into the phase field model developed by Huang and Gao [44] to numerically model the phenomenon of hydrogen embrittlement. We first briefly review the phase field model, followed by the derivation of the hydrogen diffusion equation and a proposed trapping density function to include the effect of the crack phase field value. Hydrogen embrittlement modeling considers two mechanisms. The HELP mechanism is modeled by decreasing the local flow stress with hydrogen concentration, and the HEDE mechanism is modeled by reducing the critical energy release rate with hydrogen concentration. Finally, a compact tension specimen and a flat specimen with a double notch are used to demonstrate the numerical model, and the simulation results are presented and discussed.

Phase field model

The phase field model presented by Huang and Gao is modified in this study. Detailed descriptions of this model can be found in Ref. [44]. In the framework of the phase field method, the crack surface is modeled in a diffusive manner using a field variable $d \in (0, 1)$, with $d = 0$ indicating the unbroken state while $d = 1$ indicating the broken state. The phase field value is calculated by solving the weak form of the equilibrium equation

$$\int_{\Omega} \left[-d + l^2 \Delta d + 2(1-d)H \right] dV = 0, \tag{1}$$

where Δ is the Laplacian operator, l indicates the length scale of the crack surface, H is the crack driving force defined as $H = \max \tilde{H}(\boldsymbol{x}, s)$ in loading period $s \in [0, t]$, and

$$\tilde{H} = \frac{\Psi^{e+}}{G_c / lA}, \tag{2}$$

where Ψ^{e+} is the positive part of the stored elastic energy density, G_c is the critical energy release rate, and A is a function accounts for a plastic adjustment. The value of $\tilde{H}(\boldsymbol{x}, s)$ is calculated according to the current loading step time s and the current position $\boldsymbol{x}$. The positive part of the stored elastic energy density Ψ^{e+} is defined as

$$\Psi^{e+} = K \text{tr}(\boldsymbol{\varepsilon})_+^2 + 2\mu \left(\boldsymbol{\varepsilon}_{\text{dev}}^e : \boldsymbol{\varepsilon}_{\text{dev}}^e \right), \tag{3}$$

where K represents the bulk modulus, the bracket $x_{\pm} = (x \pm |x|)/2$, μ represents the shear modulus, $\text{tr}(\boldsymbol{\varepsilon})$ represents the trace of the elastic strain tensor, $\boldsymbol{\varepsilon}_{\text{dev}}^e = \boldsymbol{\varepsilon}^e - \text{tr}(\boldsymbol{\varepsilon})I/3$ is the elastic part of the deviatoric strain tensor, and I represents the second order identity tensor.

The plastic adjustment function, A, is expressed as

$$A = \exp\left(\frac{\alpha \bar{\varepsilon}^p}{\varepsilon_f} \right), \tag{4}$$

where α is a constant coefficient, $\bar{\varepsilon}^p$ represents the effective plastic strain, and ε_f is the failure strain.

The degradation function used to describe the continuously broken process of the material is defined as

$$g(d) = (1-d)^2, \tag{5}$$

and both the Young's modulus and the yield surface are assumed to deteriorate with the increasing phase field value. Based on this assumption, the yield function is modified as

$$f(\bar{\sigma}, d, \bar{\varepsilon}^p) = g(d)\bar{\sigma} - g(d)\sigma_y(\bar{\varepsilon}^p), \tag{6}$$

where $\bar{\sigma}$ represents the equivalent stress, and σ_y represents the current yield stress.

Hydrogen transport coupled with deformation and phase field

Governing equation of hydrogen diffusion

The dissolved hydrogen atoms in most metals can either be trapped at the reversible trapping sites or diffuse between the normal interstitial lattice sites (NILS). Thus, they are divided into two populations, lattice hydrogen and trapped hydrogen, and the total hydrogen concentration is the sum of two parts

$$C = C_L + C_T = \beta_L \theta_L N_L + \beta_T \theta_T N_T, \tag{7}$$

where C_L represents the lattice hydrogen concentration, C_T represents the trapped hydrogen concentration, β_L is the number of lattice sites per solvent atom, β_T is the number of sites per trap, θ_L represents the occupancy of the lattice sites, θ_T represents the occupancy of the trapping sites, N_L represents the number of solvent atoms per unit lattice volume, and N_T represents the density of the trapping sites.

The lattice hydrogen concentration and trapped hydrogen concentration follow an equilibrium relation. The local equilibrium relation between lattice hydrogen and trapped hydrogen is expressed as [3].

$$\frac{\theta_T}{1 - \theta_T} = \frac{\theta_L}{1 - \theta_L} \exp\left(\frac{W_B}{R\Theta} \right), \tag{8}$$

where Θ represents the absolute temperature, R represents the gas constant, and W_B represents the binding energy of the trapping sites.

Consider a domain Ω with surface $\partial\Omega$, the local balance equation of total hydrogen is

$$\int_\Omega (\dot{C}_L + \dot{C}_T)\mathrm{d}V + \int_{\partial\Omega} J \cdot \mathbf{n}\mathrm{d}S = 0\,, \tag{9}$$

where $\mathbf{n}$ is the outward unit normal of the domain surface and J is the hydrogen diffusion flux. Based on Eqs. (5) and (6) and the fact that $\theta_L \ll 1$, the concentration of trapped hydrogen can be calculated by

$$C_T = \frac{\beta_T N_T}{1 + \frac{\beta_L N_L}{K_T C_L}}, \tag{10}$$

with $K_T = \exp(W_B / R\Theta)$.

Taking the time derivative of the trapped hydrogen, we can get

$$\dot{C}_T = \frac{\partial C_T}{\partial C_L}\dot{C}_L + \frac{\partial C_T}{\partial \varepsilon_p}\dot{\varepsilon}_p. \tag{11}$$

The partial derivative of the trapped hydrogen with respect to the lattice hydrogen is

$$\frac{\partial C_T}{\partial C_L} = \frac{C_T(1 - \theta_T)}{C_L}. \tag{12}$$

Taking the partial derivative of the trapped hydrogen with respect to the effective plastic strain leads to

$$\frac{\partial C_T}{\partial \varepsilon_p} = \frac{\partial C_T}{\partial N_L}\frac{\mathrm{d}N_T}{\mathrm{d}\varepsilon_p} = \theta_T \frac{\mathrm{d}N_T}{\mathrm{d}\varepsilon_p}. \tag{13}$$

Substituting Eqs. (12) and (13) into Eq. (11), we can obtain the time derivative of the trapped hydrogen as

$$\dot{C}_T = \frac{C_T(1 - \theta_T)}{C_L}\dot{C}_L + \theta_T \frac{\mathrm{d}N_T}{\mathrm{d}\varepsilon_p}\dot{\varepsilon}_p. \tag{14}$$

The total hydrogen flux J is defined as

$$J = -M_L C_L \nabla\mu_L - M_T C_T \nabla\mu_T\,, \tag{15}$$

where M_L and M_T are the mobility and μ_L and μ_T are the chemical potential of the lattice hydrogen and trapped hydrogen respectively. It is assumed that trapping sites are isolated and transport between traps is by lattice diffusion [45]. Thus, the mobility of trapped hydrogen M_T is assumed to be zero. Moreover, the mobility of the hydrogen in lattice sites M_L is assumed to degrade with the occurrence of facture. With these assumptions, the total hydrogen diffusion flux J becomes

$$J = -(1 - d)^2 M_L C_L \nabla\mu_L. \tag{16}$$

Here the degradation function is incorporated into the hydrogen diffusion flux function, which means that when the material is fully broken ($d = 1$), there is no hydrogen diffusion along or cross the newly developed crack surfaces.

The chemical potential of the lattice hydrogen is

$$\mu_L = \mu_L^0 + R\Theta\ln\left(\frac{C_L}{N_L}\right) - V_H\sigma_H\,, \tag{17}$$

where σ_H is the hydrostatic stress defined as by $\sigma_H = (\sigma_{11} + \sigma_{22} + \sigma_{33})/3$. From Eqs. (16) and (17), we can obtain

$$J = -(1 - d)^2 D_L \nabla C_L + \frac{(1 - d)^2 D_L C_L V_H}{R\Theta}\nabla\sigma_H, \tag{18}$$

where the lattice diffusion coefficient $D_L = M_L R\Theta$. Substituting Eqs. (14) and (18) into Eq. (9) results in

$$\left\{ \begin{array}{l} \displaystyle\int_\Omega \left[\frac{C_L + C_T(1 - \theta_T)}{C_L}\dot{C}_L + \theta_T\frac{\mathrm{d}N_T}{\mathrm{d}\varepsilon_p}\dot{\varepsilon}_p\right]\mathrm{d}V + \\[2ex] \displaystyle\int_{\partial\Omega}\left[-(1 - d)^2 D_L\nabla C_L + \frac{(1 - d)^2 D_L C_L V_H}{R\Theta}\nabla\sigma_H\right]\cdot\mathbf{n}\mathrm{d}S \end{array}\right\} = 0\,. \tag{19}$$

Applying Gauss's divergence theorem results in

$$\begin{aligned} &\frac{C_L + C_T(1 - \theta_T)}{C_L}\dot{C}_L - \nabla\cdot\left[(1 - d)^2 D_L\nabla C_L\right] \\ &+ \nabla\cdot\left[\frac{(1 - d)^2 D_L C_L V_H}{R\Theta}\nabla\sigma_H\right] + \theta_T\frac{\mathrm{d}N_T}{\mathrm{d}\varepsilon_p}\dot{\varepsilon}_p = 0. \end{aligned} \tag{20}$$

This is the governing equation for hydrogen transport that takes into account the effect of the crack phase field. From Eq. (20) we can see that the diffusion of lattice hydrogen is not only affected by the gradient of lattice hydrogen concentration, but also affected by the trapped hydrogen concentration, the gradient of hydrostatic stress, the plastic deformation, and the phase field value.

Hydrogen trapping

In Eq. (7), the trapped hydrogen concentration is a function of the occupancy of the trapping sites θ_T, the number of sites per trap β_T, and the trapping density N_T. Here β_T is a material constant, and θ_T is a factor for the equilibrium relation between trapped hydrogen and lattice hydrogen. As for the trapping density N_T, Kumnick and Johnson [46] showed that in iron, it is associated with dislocations developed during plastic deformation. Sofronis and McMeeking [4] suggested that in BCC iron, the trapping density N_T increases monotonically with the increased plastic strain and it is independent of temperature. They also assumed that the trapping density saturates as the plastic strain becomes larger than 0.8. According to the experimental observations presented by Kumnick and Johnson [46], Taha and Sofronis [47] proposed that for iron and steels, the trapping density is a function of the plastic strain, and the relation is written as follows

$$\log(N_T) = 23.26 - 2.33\exp(-5.5\bar{\varepsilon}^p). \tag{21}$$

Atomistic simulations [48] show that as a crack propagates through a hydrogen-rich region, the hydrogen atoms are trapped along the newly created crack surfaces, and behind the new crack tip hydrogen concentration does not increase. However, in the phase field model, the crack topology is represented in a diffusive manner using the phase field value, d, and the plastic strain in the area of the diffusive crack still increases monotonically after fracture occurred, resulting in a monotonic increase in trapping density there according to Eq. (21). To overcome this problem, we propose a new trapping density function in an incremental form as follows

$$\log(N_T) = 23.26 - 2.33\exp(-5.5\tilde{\varepsilon}^p). \tag{22}$$

Different from (21), here the plastic factor $\tilde{\varepsilon}^p$ is not the effective plastic strain, but a function of the effective plastic

strain and the crack phase field value. At time increment $n+1$, the plastic factor is defined as $\tilde{\varepsilon}_{n+1}^{p} = \tilde{\varepsilon}_{n}^{p} + (1 - d_{n+1})^2 \Delta \bar{\varepsilon}^{p}$.

Hydrogen embrittlement modeling

Various mechanisms contribute to hydrogen induced cracking, among which the HELP and HEDE mechanisms are incorporated into the phase filed model in this study. Birnbaum and Sofronis [14] suggested that dissolved hydrogen atoms in steels promote the mobility of dislocation, thus decrease the local yield stress. Sofronis et al. [49] and Liang et al. [50] proposed a HELP model that assumed the yield stress to be a function of the hydrogen concentration and the plastic strain to phenomenologically describe the HELP effect as

$$\sigma_y(\varepsilon_p, c) = \sigma_0(c)\left(1 + \frac{\varepsilon_p}{\varepsilon_0}\right)^N, \tag{23}$$

with

$$\sigma_0(c) = \begin{cases} \left[(\vartheta - 1)\dfrac{c}{c_0}\right]\sigma_0 & \sigma_0(c) > \eta\sigma_0 \\ \eta\sigma_0 & \sigma_0(c) \le \eta\sigma_0 \end{cases}, \tag{24}$$

where c represents the hydrogen concentration, $\sigma_0(c)$ represents the initial yield stress with the HELP effect, E is the Young's modulus, $\varepsilon_0 = \sigma_0/E$ with $\sigma_0 = \sigma_0$ (0) indicating the initial yield condition with no presence of hydrogen, N represents the strain hardening exponent, ε_p is the plastic strain, ϑ is a softening parameter, and $\eta\sigma_0$ represents the lower bound of the yield stress with η having a constant value between 0 and 1, indicating the maximum HELP effect on the yield stress.

The HEDE effect is a result of the reduced bonding energy between metal atoms and is often reflected by the reduction of cohesive strength along the grain boundaries [51], the fracture mechanism transition from ductile to brittle [28], and the reduction of surface energy. Here a phenomenological model is used to account for the HEDE effect, in which the critical energy release rate is assumed to be a decreasing function of the hydrogen concentration

$$\bar{G}_c = G_c(c), \tag{25}$$

and the function $G_c(c)$ is assumed to take the form of

$$G_c(c) = \begin{cases} \left[(\zeta - 1)\dfrac{c}{c_0}\right]G_c & G_c(c) > \xi G_c \\ \xi G_c & G_c(c) \le \xi G_c \end{cases}, \tag{26}$$

where ζ and ξ are parameters controlling the reduction of the critical energy release rate, with ξG_c being a lower bound value. It is worth pointing out that Eq. (26) is not derived from experimental data nor from atomistic simulations. It is rather to provide a simple model to account for the effect of hydrogen on the critical energy release rate phenomenologically. Note that Eqs. (24) and (26) have similar forms. With the definition of $\bar{G}_c$, the crack driving force function given by Eq. (2) now can be expressed as

$$\tilde{H} = \frac{\Psi^{e+}}{\bar{G}_c/lA}. \tag{27}$$

Constitutive equations

Huang and Gao [44] adopted the von Mises plasticity theory in their phase field model. They assumed that only the deviatoric part of the total stress and the tensile part of the volumetric stress are degraded as the phase field value increases. Therefore, the stress tensor can be calculated by

$$\boldsymbol{\sigma} = [1 - H(\varepsilon_{kk})d]^2 K\varepsilon_{kk}\mathbf{I} + 2(1 - d)^2 \mu\boldsymbol{\varepsilon}_{dev}^{e}, \tag{28}$$

where $H(\varepsilon_{kk})$ represents the Heaviside function. And in time interval $[t_n, t_{n+1}]$, the trial elastic strain tensor is calculated by

$$\boldsymbol{\varepsilon}_{n+1}^{e\ trial} = \boldsymbol{\varepsilon}_n^{e} + \Delta\boldsymbol{\varepsilon}, \tag{29}$$

where $\boldsymbol{\varepsilon}_n^{e}$ is the elastic strain tensor updated at the end of the increment n and $\Delta\varepsilon$ indicates the total strain increment tensor at increment $n + 1$. Then, the volumetric elastic trail stress tensor $\mathbf{p}_{n+1}^{e\ trial}$ and the deviatoric elastic trial stress tensor $\mathbf{s}_{n+1}^{e\ trial}$ are expressed as

$$\begin{aligned} \mathbf{p}_{n+1}^{e\ trial} &= \left[1 - H(\varepsilon_{kk\ n+1}^{e\ trial})d\right]^2 K\varepsilon_{kk\ n+1}^{e\ trial}\mathbf{I}; \\ \mathbf{s}_{n+1}^{e\ trial} &= 2(1 - d)^2 \mu\boldsymbol{\varepsilon}_{dev\ n+1}^{e\ trial}, \end{aligned} \tag{30}$$

The return-mapping algorithm is used to integrate the plastic rate equation, details can be found in Ref. [44].

Yield function

To incorporate the HELP effect in the phase field model, Eq. (24) should be combined with Eq. (6). Therefore, the yield condition becomes a function of the hydrogen concentration, the phase field value and the effective plastic strain

$$f(\bar{\sigma}, c, d, \bar{\varepsilon}^p) = \bar{\sigma}(d) - \sigma_y(c, d, \bar{\varepsilon}^p). \tag{31}$$

The proposed form of the yield function is expressed as

$$f(\bar{\sigma}, c, d, \bar{\varepsilon}^p) = g(d)\bar{\sigma} - s(c)g(d)\sigma_y(\bar{\varepsilon}^p), \tag{32}$$

where $g(d)$ is the degradation function as defined in Eq. (5), and $s(c)$ is the softening function similar to Eq. (24)

$$s(c) = \begin{cases} \left[(1 - \vartheta)\dfrac{c}{c_0}\right] & s(c) > \eta \\ \eta & s(c) \le \eta \end{cases}. \tag{33}$$

Here ϑ and η are the same as in Eq. (24). Noted that $s(c)$ is a dimensionless softening factor.

Numerical implementation

A user subroutine UEL for a commercial finite element software ABAQUS is developed to implement the modified phase field model, with the phase field value treated as the degrees

of freedom #11. Details of the numerical procedure is described in Ref. [44]. The hydrogen diffusion governing equation is solved using an ABAQUS user subroutine UMATHT [21]. A common block is used to pass variables between UEL and UMATHT.

The HELP effect is included in the phase field model by taking into account the hydrogen effect on the yield stress as described in Eqs. (32) and (33). The HEDE effect is included in the phase filed model by varying the critical energy release rate according to Eqs. (25) and (26). A previous study by Huang et al. [21] suggests that HELP embrittles ductile materials by accelerating the growth of micro-voids, and another study by Huang and Gao [44] suggests that lowering the critical energy release rate reduces material's strength as well as ductility. In the present hydrogen embrittlement model, both HELP and HEDE are accounted for. To demonstrate the proposed model, numerical simulations of a compact tension (CT) specimen and a double notched flat specimen are conducted for four cases: 1) no HELP or HEDE effect, 2) only HELP effect, 3) only HEDE effect, and 4) with both HELP and HEDE effects. Both specimens are under displacement-control. The loading speeds are set to be slow enough to ensure sufficient time for lattice hydrogen diffusion so that the hydrogen concentration field remains steady state during the loading process. Assume a uniformly initial hydrogen distribution in both specimens with the initial value $C_L = 2.084 \times 10^{12}$ atoms/mm^3, and the trapped hydrogen concentration C_T is calculated according to the equilibrium relation. The "no flux boundary condition" is imposed on the exterior surfaces of both specimens. Hydrogen redistribution in the specimen is driven by the varying stress and deformation fields. The material's mechanical properties and parameters for hydrogen diffusion are listed in Table 1 [21,44]. The length scale is assumed to be $l = 1.0$ mm. The numerical results of the CT specimen are presented and discussed first in the next section, followed by the results of the double notched specimen.

Compact tension specimen

In this section, simulations of a CT specimen are conducted and the numerical results are discussed. Fig. 1(a) shows the dimensions (in mm) of the CT specimen having a thickness of 2.5 mm. Fig. 1(b) displays the finite element mesh showing refined mesh in the region where fracture is expected to occur. The minimum element size is 0.25 mm. Results of hydrogen diffusion and hydrogen trapping of the case with no HELP or HEDE effect are presented and discussed first, followed by the di scussion of the effects of HELP and HEDE on hydrogen embrittlement.

Lattice hydrogen diffusion and hydrogen trapping

Fig. 2 shows the distributions of crack phase field value and lattice hydrogen concentration on the mid-surface of the specimen just before the onset of crack initiation. The lattice hydrogen concentration is high in the area ahead of the crack tip as a result of high positive hydrostatic stress in this area. As the phase field values reaches one, crack starts to propagate. During crack propagation, the area of high positive

Table 1 – Material parameters.		
Properties	Values	Units
Young's modulus	$E = 200$	GPa
Possion's ratio	$v = 0.3$	–
Yield stress	$\sigma_y = 500$	MPa
Hardening modulus	$h = 100$	MPa
Critical energy release rate	$G_c = 20$	mJ/mm^2
Fracture strain	$\varepsilon_f = 0.05$	–
Coefficient α	$\alpha = 8$	–
Diffusion coefficient	$D_L = 0.0127$	mm^2/s
Molar volume of iron	$V_M = 7160$	mm^3/mol
Lattice site density	$N_L = 8.46 \times 10^{19}$	atoms/mm^3
Molar volume of hydrogen in solid solution	$V_H = 2000$	mm^3/mol
Binding energy	$W_B = 60$	kJ/mol
Number of NILS per solvent atom	$\beta_L = 6$	–
Number of sites per trap	$\beta_T = 1$	–

hydrostatic stress moves with the crack tip [44]. Fig. 3 shows the distributions of crack phase field value and lattice hydrogen concentration on the mid-surface of the specimen after some amount of crack propagation. The red color in Fig. 3(a) represents the new crack surfaces. Fig. 3(b) shows the area of high lattice hydrogen distribution moves to the new crack tip where positive hydrostatic stress exists. These results are in accord with experimental observations by previous researchers [52,53].

Figs. 4 and 5 show the distributions of crack phase field value, trapped hydrogen concentration and total hydrogen concentration prior to and after fracture initiation respectively. Here Figs. 4(a) and 5(a), showing the crack phase field distributions, are the same as Figs. 2(a) and 3(a) respectively, whose purpose is to indicate the crack tip location. Prior to the onset of crack initiation, trapped hydrogen is concentrated in a small region ahead of the crack tip where plastic deformation takes place, Fig. 4(b). After crack starts propagating, more hydrogen is trapped along the newly created crack surfaces as shown in Fig. 5(b). This agrees with the atomistic simulation result [48] that trapped hydrogen atoms tend to stay on the newly created crack surfaces.

Fig. 4(c) shows the distribution of total hydrogen concentration (lattice hydrogen plus trapped hydrogen) prior to crack initiation, where the hydrogen concentration is the highest at the crack tip region. Fig. 5(c) shows the distribution of total hydrogen concentration ahead of the crack tip after some amount of crack propagation. Note that in Fig. 5(c), fractured elements with phase field value equal to one are removed from the picture, which is for the purpose of a better illustration of the total hydrogen concentration in the material. Fig. 5(c) indicates that hydrogen keeps transporting to and being trapped in the area ahead of the growing crack tip.

It is worth mentioning that by comparing the crack tip hydrogen concentrations shown in Figs. 4(c) and 5(c), it is noticed that the total hydrogen concentration at the crack tip region decreases as crack propagates. This is because the total amount of hydrogen is fixed in the simulation (no flux boundary condition on the exterior surfaces) and more hydrogen is trapped along the newly created crack surfaces as crack propagates. This result agrees with the atomistic simulation result by Song and Curtin [37].
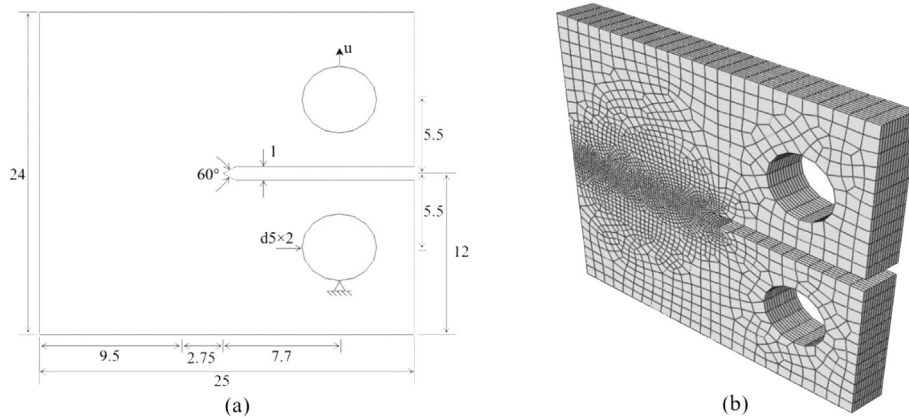
Fig. 1 – (a) Dimensions (in mm) of a CT specimen. (b) Finite element mesh of the CT specimen.
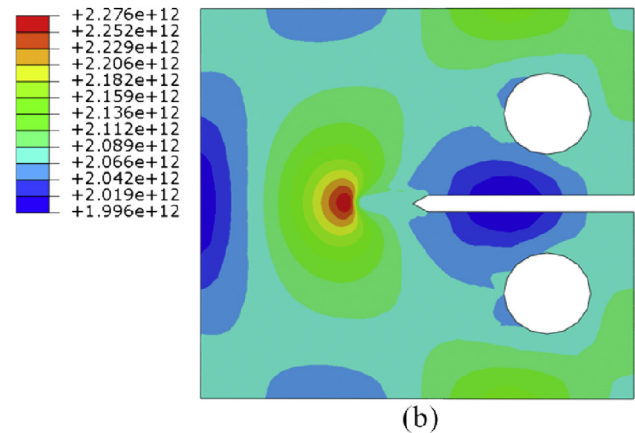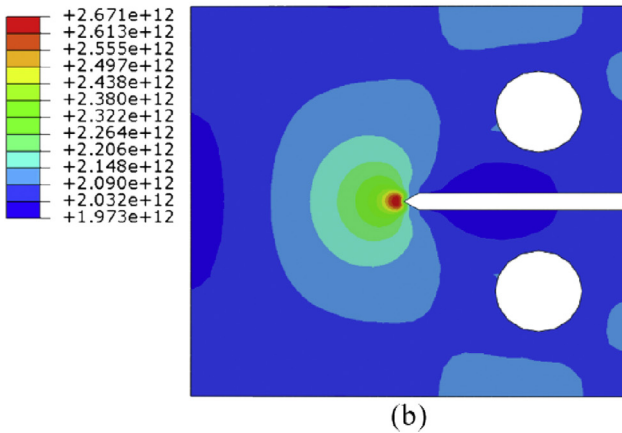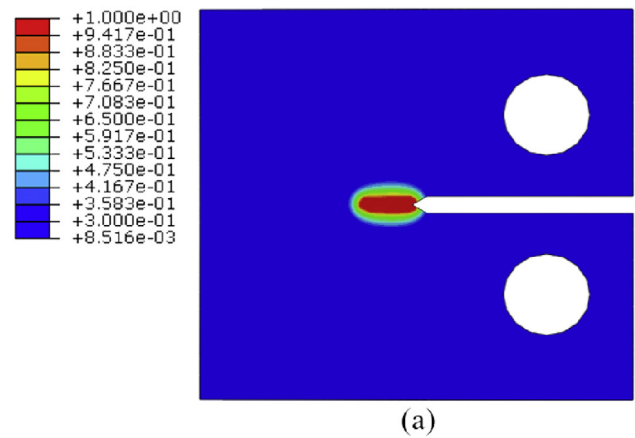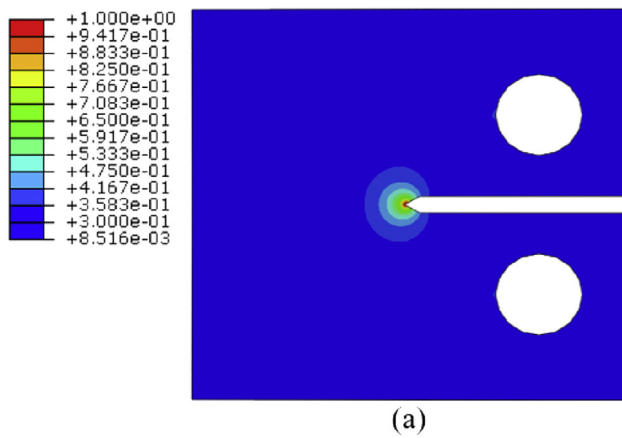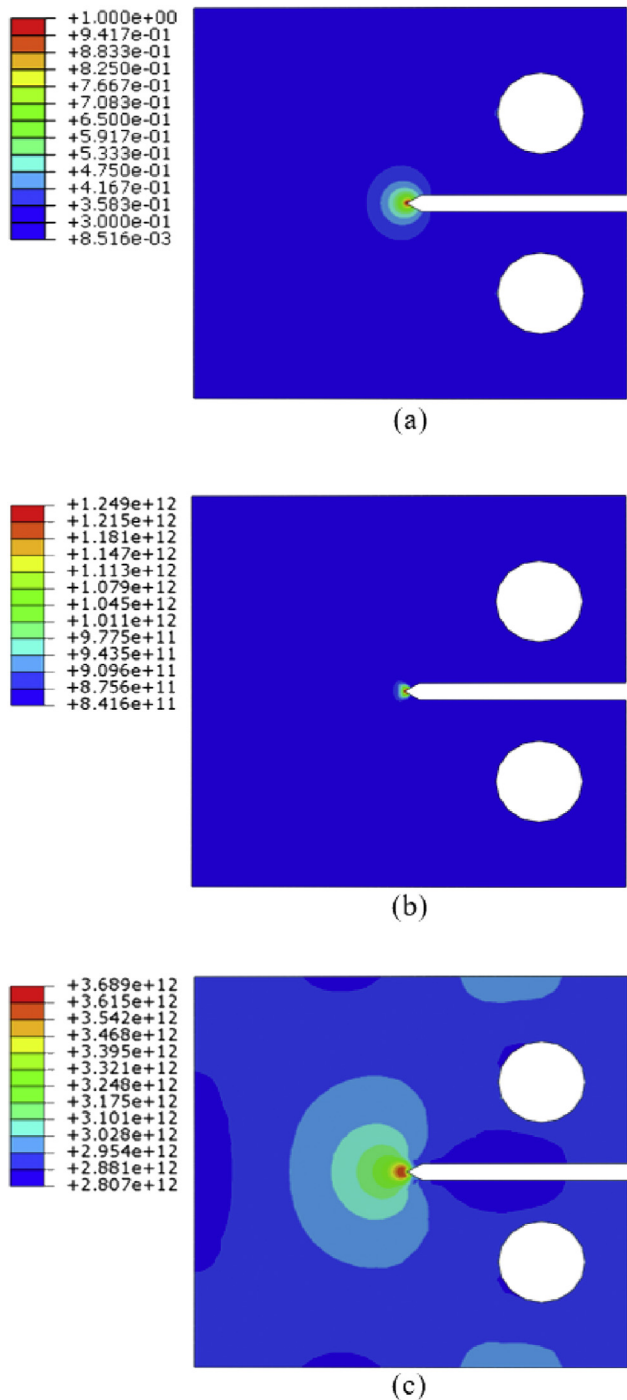

Fig. 2 – Distributions of crack phase field value (a) and lattice hydrogen concentration (b) on the mid-surface of the specimen before the onset of crack initiation.

Fig. 3 – Distributions of rack phase field values (a) and lattice hydrogen concentration (b) on the mid-surface of the specimen after some amount of crack propagation.

The simulation results presented above confirms that the numerical model is capable of capturing the hydrogen diffusion and hydrogen trapping mechanisms and correctly simulating the hydrogen transport phenomenon. Coupling the hydrogen concentration with the HELP and HEDE mechanisms, parameters affecting hydrogen embrittlement can be analyzed and discussed.

Hydrogen embrittlement mechanisms

To demonstrate the influence of HELP and HEDE on hydrogen embrittlement, four cases, 1) no HELP or HEDE effect, 2) only HELP effect, 3) only HEDE effect, and 4) with both HELP and HEDE effects, are analyzed and compared. Case 1 serves as a baseline for comparison. The HELP effect on the yield stress is

Fig. 4 – Distributions of crack phase field value (a), trapped hydrogen concentration (b), and total hydrogen concentration (c) on the mid-surface of the specimen prior to fracture initiation.


Fig. 5 – Distributions of crack phase field value (a), trapped hydrogen concentration (b), and total hydrogen concentration (c) on the mid-surface of the specimen after some amount of crack propagation.

defined by Eq. (32), and the values of ϑ and η are set to be 0.9 and 0.5 respectively. The HEDE effect on the critical energy release rate is defined by Eq. (26), and the values ζ and ξ are also set to be 0.9 and 0.5 respectively. Fig. 6 compares the load-displacement curves (solid lines) for the four cases. The variations of the maximum plastic strain during the loading history (dashed lines) for the four cases are also shown in Fig. 6.
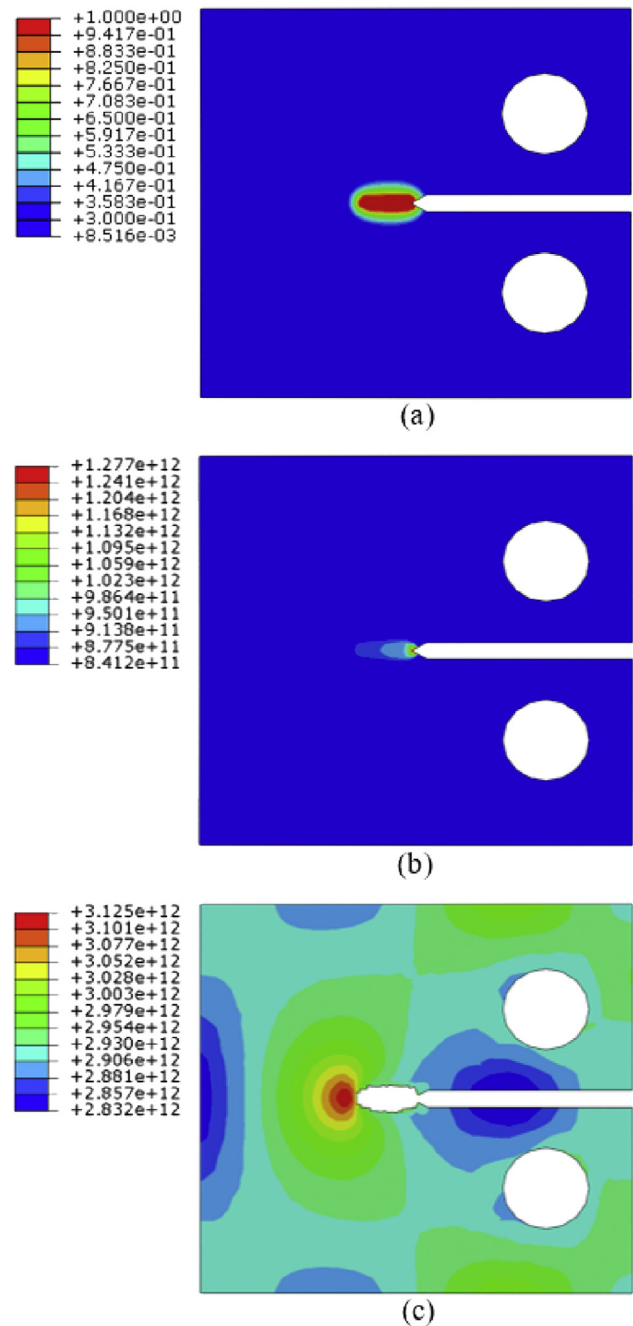
Comparing the result of case 2, which includes only the HELP effect, to the baseline case, where neither HELP nor HEDE effect is considered, the results show that HELP reduces the load carrying capacity of the specimen, i.e., it reduces the strength and fracture toughness of the material. Moreover, HELP leads to more plastic deformation in the specimen as reflected by a higher value of plastic strain at the same applied displacement in the maximum plastic strain-displacement curve. These results agree with previous findings of the HELP effect on ductile fracture [19,21]. Comparing the result of
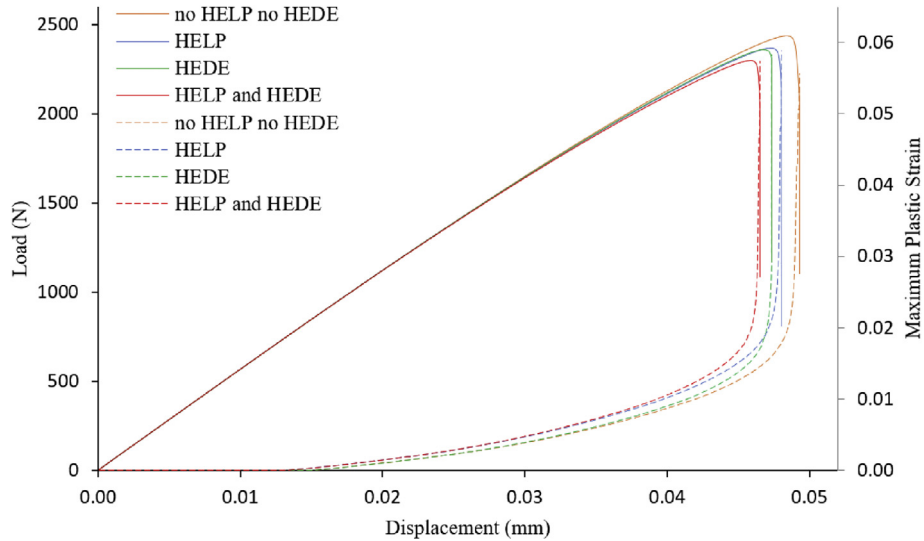
Fig. 6 – Load-displacement curves (solid lines) and maximum plastic strain-displacement curves (dashed lines) for different cases, where the HELP parameters are $\vartheta = 0.9$ and $\eta = 0.5$, and the HEDE parameters are $\zeta = 0.9$ and $\xi = 0.5$.
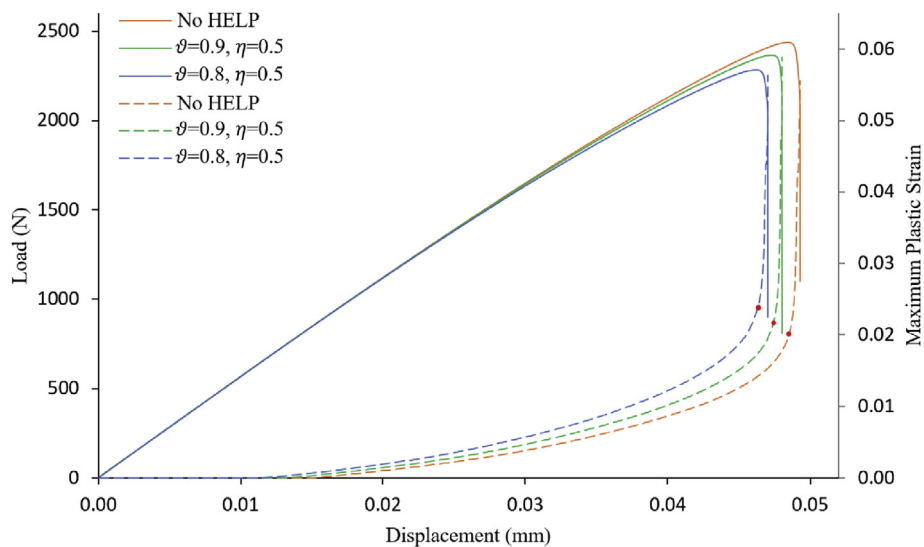
Fig. 7 – Load-displacement curves (solid lines) and maximum plastic strain-displacement curves (dashed lines) obtained with different HELP parameters.

case 3, which includes only the HEDE effect, with the baseline case, it is seen that the HEDE effect also lowers the strength and ductility of the material, however there is no noticeable difference between the maximum plastic strain-displacement curves of the two cases before crack initiation. With both HELP and HEDE mechanisms included in the simulation, case 4 exhibits the lowest load carrying capacity.

To further discuss the HELP effect, simulations are conducted with different values of parameter ϑ. Fig. 7 compares the results obtained from three cases: ($\vartheta = 0.9$; $\eta = 0.5$), ($\vartheta = 0.8$; $\eta = 0.5$), and the baseline case. The sudden drop of the load-displacement curve indicates the onset of crack propagation. The red dots on the dashed lines represent the maximum plastic strain values when the crack start to propagate. Fig. 7 shows that with only HELP effect, the load

carrying capacity decreases as the value of ϑ decreases. In addition, the maximum value of plastic strain at fracture initiation is higher when the HELP effect is considered, and it increases as the value of ϑ decreases.

Similarly, to further discuss the HEDE effect, simulations are conducted with different values of parameter ζ. Fig. 8 compares the results obtained from three cases: ($\zeta = 0.9$; $\xi = 0.5$), ($\zeta = 0.8$; $\xi = 0.5$), and the baseline case. With only HEDE effect, the load carrying capacity decreases as the value of ζ decreases. In addition, the maximum value of plastic strain at fracture initiation is lower when the HEDE effect is considered, and it decreases as the value of ζ decreases.
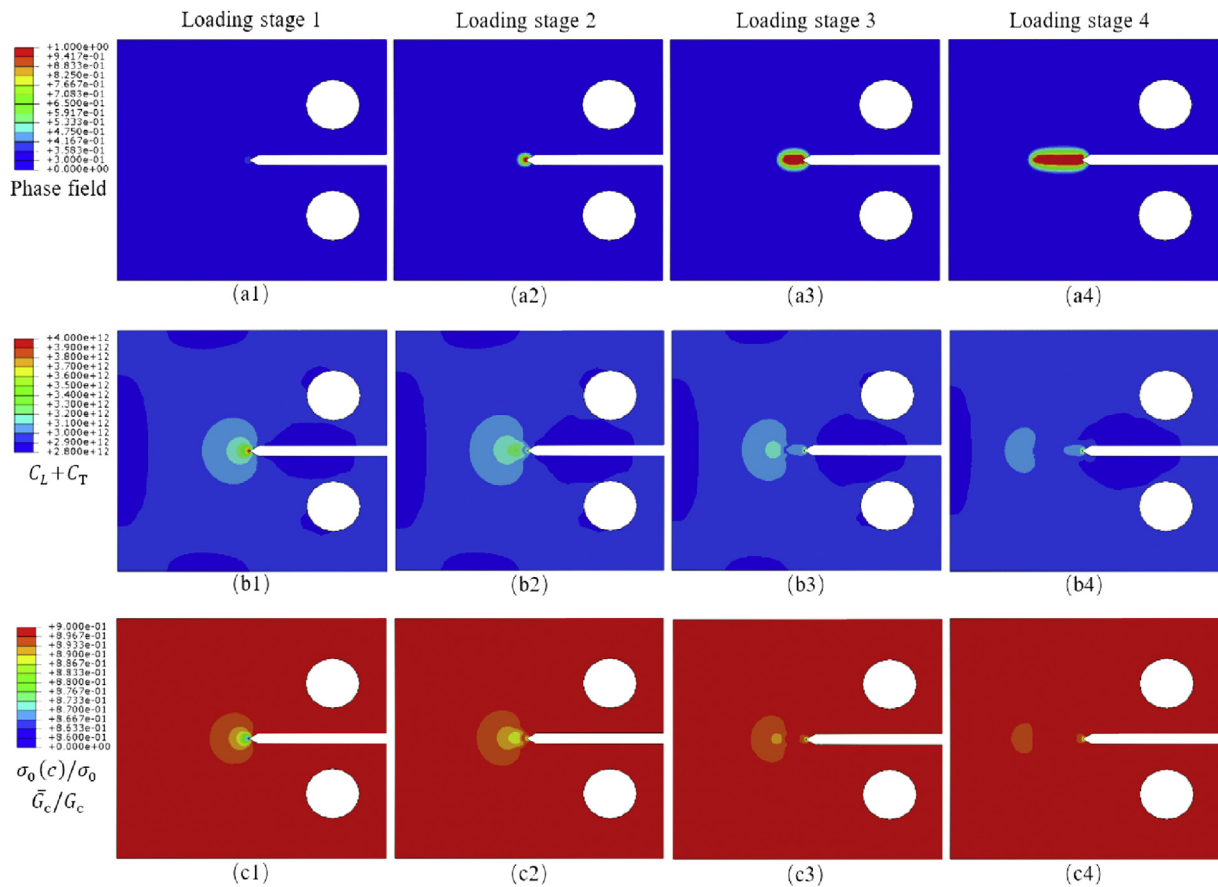
Fig. 9 compares the hydrogen embrittlement effects (HELP and HEDE mechanisms) at different loading stages. The HELP and HEDE effects are evaluated by the values of $\sigma_0(c)/\sigma_0$ and
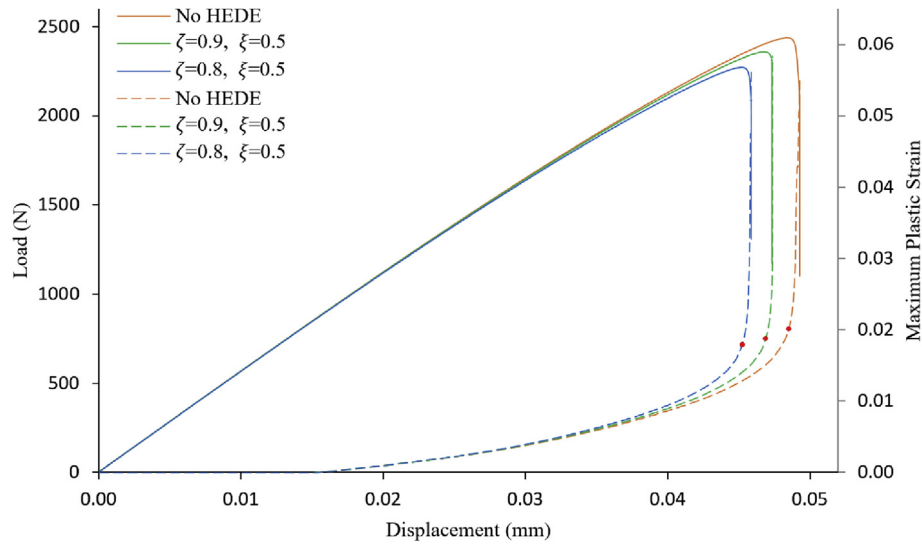
Fig. 8 − Load-displacement curves (solid lines) and maximum plastic strain-displacement curves (dashed lines) obtained with different HEDE parameters.

$G_c(c)/G_c$ respectively. The values of $\sigma_0(c)/\sigma_0$ and $G_c(c)/G_c$ are the same because the values of the parameters used to describe the HELP and HEDE effects are the same ($\vartheta = \zeta = 0.9$ and $\eta = \xi = 0.5$). Fig. 9(a1−a4) show the distribution of the crack phase field value at four different loading stages, with

the red color represents the newly created crack. Fig. 9(b1−b4) show the distribution of the total hydrogen concentration at the four loading stages. The peak hydrogen concentration is at the crack tip and its value is decreasing from loading stage 1 to loading stage 4 because of the no hydrogen diffusion flux

Fig. 9 − Distributions of crack phase field value (a1−a4), total hydrogen concentration (b1−b4), and hydrogen embrittlement effects (c1−c4) on the mid-surface of the specimen at different loading stages (number 1−4 in each row).
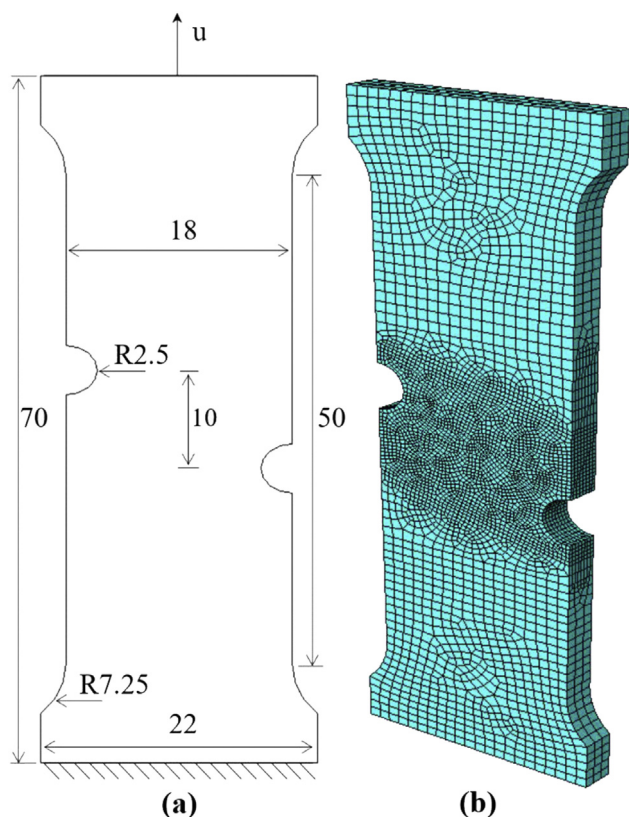
Fig. 10 – (a) Dimensions of a flat specimen with double notches (in mm); (b) finite element mesh.

boundary condition and more hydrogen being trapped along the newly created crack surfaces. As a result of the decrease of the total hydrogen, the embrittlement effect at the crack tip is weakening as the loading process continues, Fig. 9(c1–c4).

The strongest embrittlement effect takes place at the crack tip before crack starts to initiate, Fig. 9(c1), where the values of $\sigma_0(c)/\sigma_0$ and $G_c(c)/G_c$ are the lowest (~0.86). At this stage, the embrittlement effects are controlled by the accumulated hydrogen (lattice hydrogen and trapped hydrogen) at the crack tip as well as the embrittlement parameters ϑ and ζ. As loading continues and crack propagates, the values of $\sigma_0(c)/\sigma_0$ and $G_c(c)/G_c$ gradually increase to close to the initial value of 0.9 due to diminished hydrogen accumulation at the crack tip. From this stage on, the embrittlement effects are controlled only by the embrittlement parameters ϑ and ζ.

Results presented above suggest that the proposed phase field model has the ability to predict hydrogen embrittlement resulted from the HELP and HEDE mechanisms. HELP promotes the localization of plastic strain and accelerates material failure. HEDE reduces the critical energy release rate and facilitates crack propagation. The simulation results are in qualitative agreement with the previous investigations [19,21,44].

Double notched flat specimen

In this section, simulations of a flat specimen with double notches are conducted, and the results are presented to further validate the proposed numerical model. Fig. 10(a) shows the geometry of the double notched specimen having a thickness of 3 mm, and Fig. 10(b) shows the finite element mesh with the minimum element size of 0.4 mm. The material properties and hydrogen diffusion parameters are the same as those listed in Table 1, expect for a higher critical energy release rate, $G_c = 60$ mJ/mm^3, being used in simulations conducted in this section. Four cases, 1) no HELP or HEDE effect, 2) only HELP effect, 3) only HEDE effect, and 4) with both HELP and HEDE effects, are analyzed and compared.

Lattice hydrogen diffusion and hydrogen trapping

The results of hydrogen diffusion and hydrogen trapping for the baseline the case 1 (no HELP or HEDE effect) are displayed in Fig. 11. Pictures a1, b1, c1 and d1 show the distributions of the crack phase field value, the lattice hydrogen, the trapped hydrogen and the total hydrogen prior to crack propagation respectively. Pictures a2, b2, c2 and d2 show the corresponding contours after some amount of crack propagation. Similar to the results of presented in the previous section for the CT specimen, the lattice hydrogen accumulates at the notch tips prior to crack propagation, Fig. 11(b1), and the new crack tips after crack propagation, Fig. 11(b2). More hydrogen is trapped at the notch tips before crack propagation, Fig. 11(c1), and the trapped hydrogen remains on the newly created crack surfaces after crack propagation, Fig. 11(c2). The total hydrogen concentration is highest at the notch tips before fracture, Fig. 11(d1), and at the new crack tips after crack propagation, Fig. 11(d2). The peak value of total hydrogen concentration reduces as the crack propagates.

Hydrogen embrittlement mechanisms

The load-displacement curves (solid lines) and the variations of the maximum plastic strain curves (dashed lines) during the loading process of the four cases are plotted in Fig. 12, where reductions in strength and ductility caused by the HELP and HEDE effects can be observed. One difference that worth mentioning is that, in Fig. 12, the load-displacement curve of case 2 is lower and the sudden drop occurs earlier than case 3, while Fig. 6 shows an opposite trend for the CT specimen. In Fig. 12, the displacements at which the load curves drop rapidly are marked by two vertical dashed lines labeled as "loading stage 1", "loading stage 2" and "loading stage 3" for case 2 (with HELP effect), case 3 (with HEDE effect) and case 4 (with both HELP and HEDE effects) respectively. This result suggests that, for the double notched specimen, the HELP effect on the strength and ductility is stronger than the HEDE effect, while it is opposite for the CT specimen. This difference may result from not only the geometrical disparity of the notch tips in two specimens but also the higher critical energy release rate used for the simulations of a flat specimen with a double notch.

To analyze how the HELP mechanism embrittles the material, Fig. 13 compares the simulation results for case 1 (no HELP or HEDE) and case 2 (with HELP) at the loading stage 1 indicated in Fig. 12. The HELP effect results in higher plastic strain at the notch tip, Fig. 13(a1,a2), and higher plastic strain results in more trapped hydrogen, Fig. 13(b1,b2), therefore, leading to higher total hydrogen concentration at the notch tip
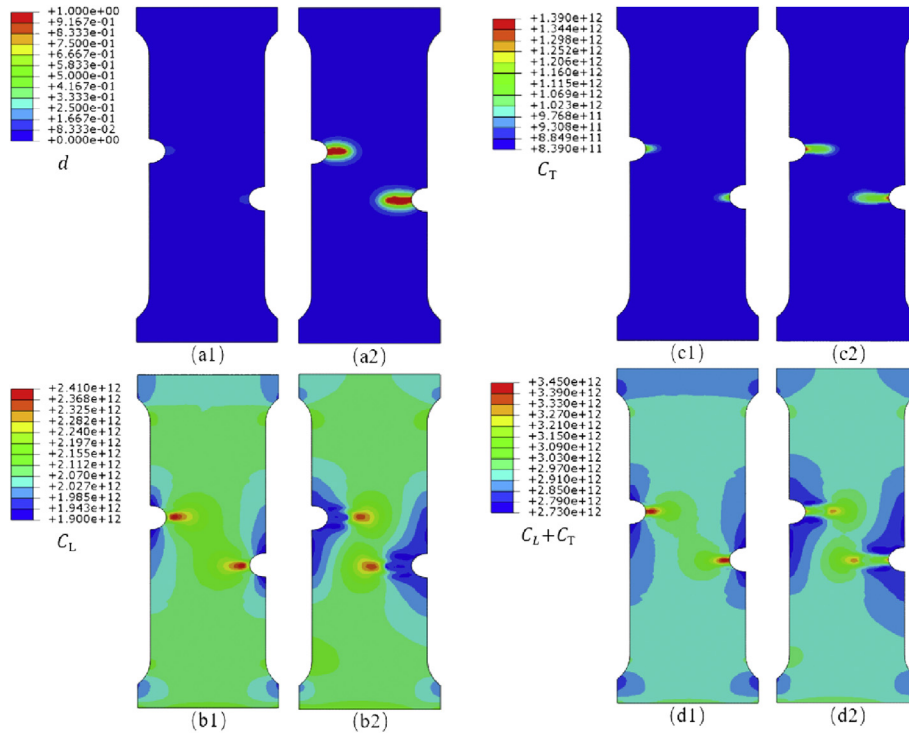
Fig. 11 – Distributions of crack phase field value (a1, a2), the lattice hydrogen (b1, b2), the trapped hydrogen (c1, c2), and the total hydrogen (d1, d2) on the mid-surface of the specimen before (a1, b1, c1, d1) and after (a2, b2, c2, d2) the onset of crack initiation.

area, Fig. 13(c1,c2). The accumulated hydrogen at the notch tip further promotes local plastic straining in this area, which in turn facilitates more hydrogen accumulation. As a consequence of this effect, crack initiation occurs faster for case 2 than case 1, Fig. 13(d1,d2).

Fig. 14 examines the HEDE mechanism by comparing the simulation results for case 1 (no HELP or HEDE) and case 3 (with HEDE) at the loading stage 2 indicated in Fig. 12. As shown in Fig. 14(a1,a2,b1,b2), the HEDE mechanism also facilitates plastic straining and promotes hydrogen trapping at
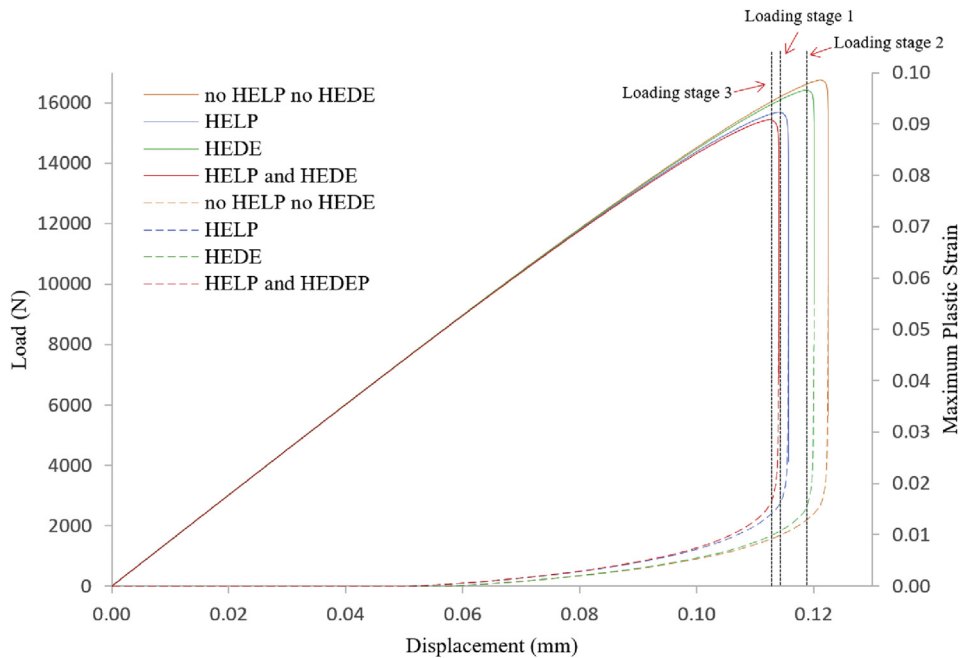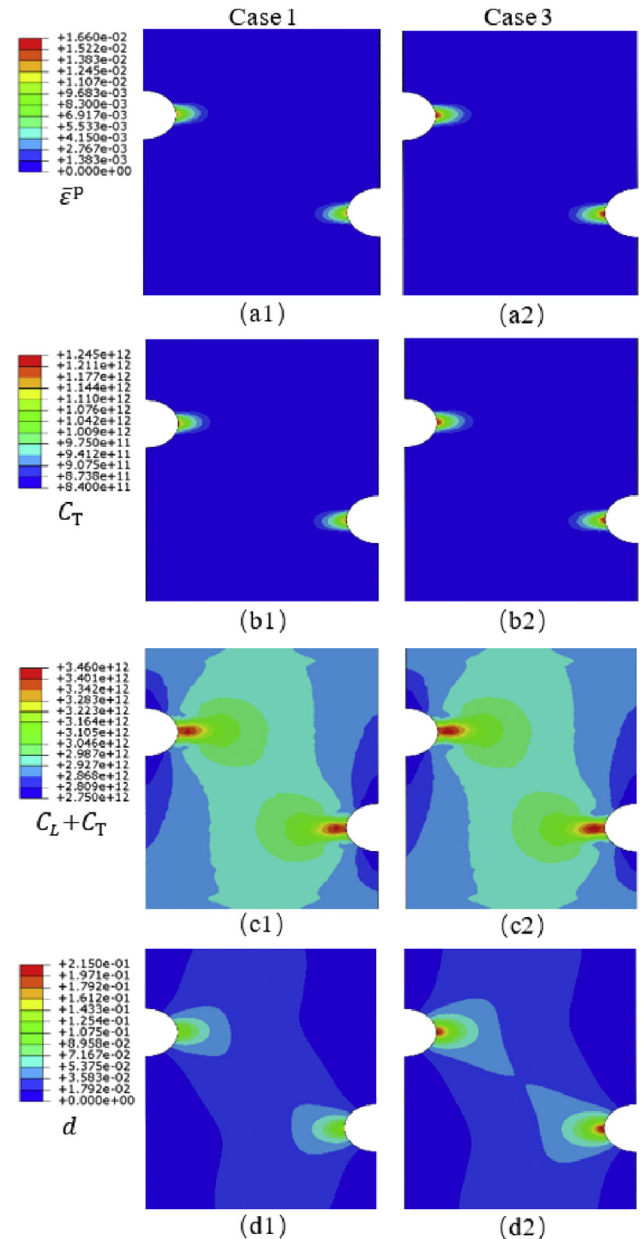

Fig. 12 – Load-displacement curves (solid lines) and maximum plastic strain-displacement curves (dashed lines) for different cases, where the HELP parameters are $\vartheta = 0.9$ and $\eta = 0.5$, and the HEDE parameters are $\zeta = 0.9$ and $\xi = 0.5$.
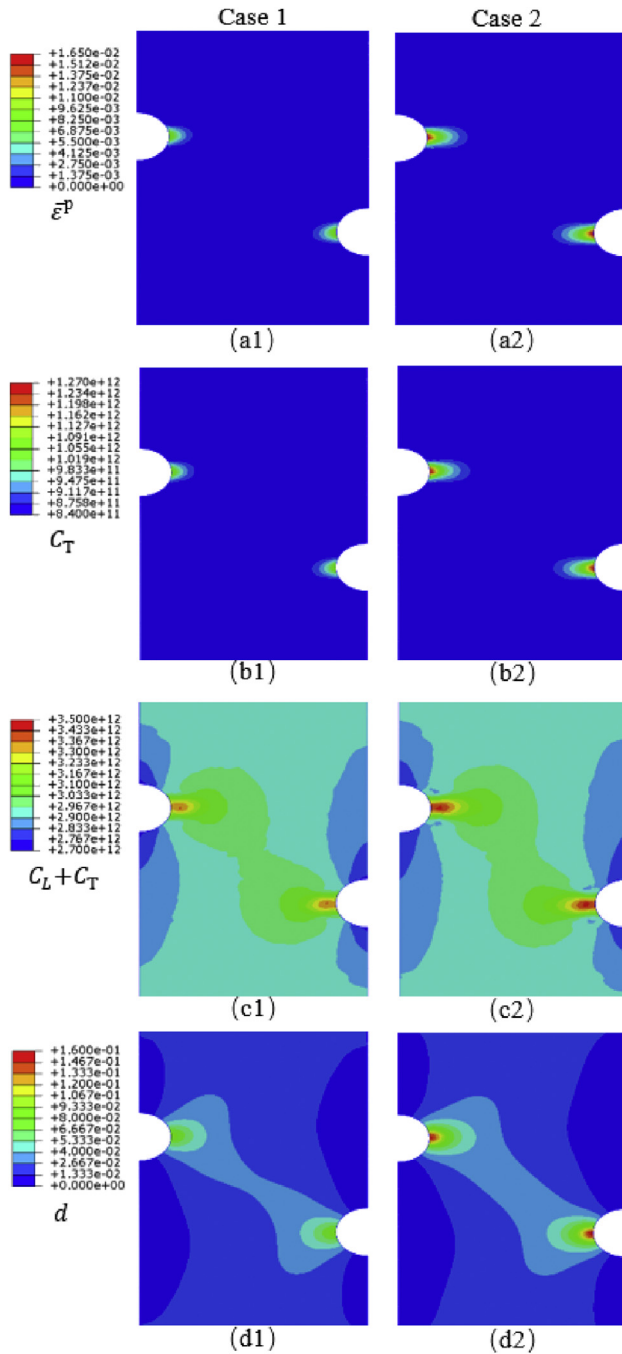
Fig. 13 — Distributions of the effective plastic strain (a1, a2), the trapped hydrogen (b1, b2), the total hydrogen (c1, c2) and the crack phase field value (d1, d2) on the mid-surface of the specimen for case 1 (a1, b1, c1, d1) and case 2 (a2, b2, c2, d2) at the loading stage 1 indicated in Fig. 12.

Fig. 14 — Distributions of the effective plastic strain (a1, a2), the trapped hydrogen (b1, b2), the total hydrogen (c1, c2) and the crack phase field value (d1, d2) on the mid-surface of the specimen for case 1 (a1, b1, c1, d1) and case 3 (a2, b2, c2, d2) at the loading stage 2 indicated in Fig. 12.
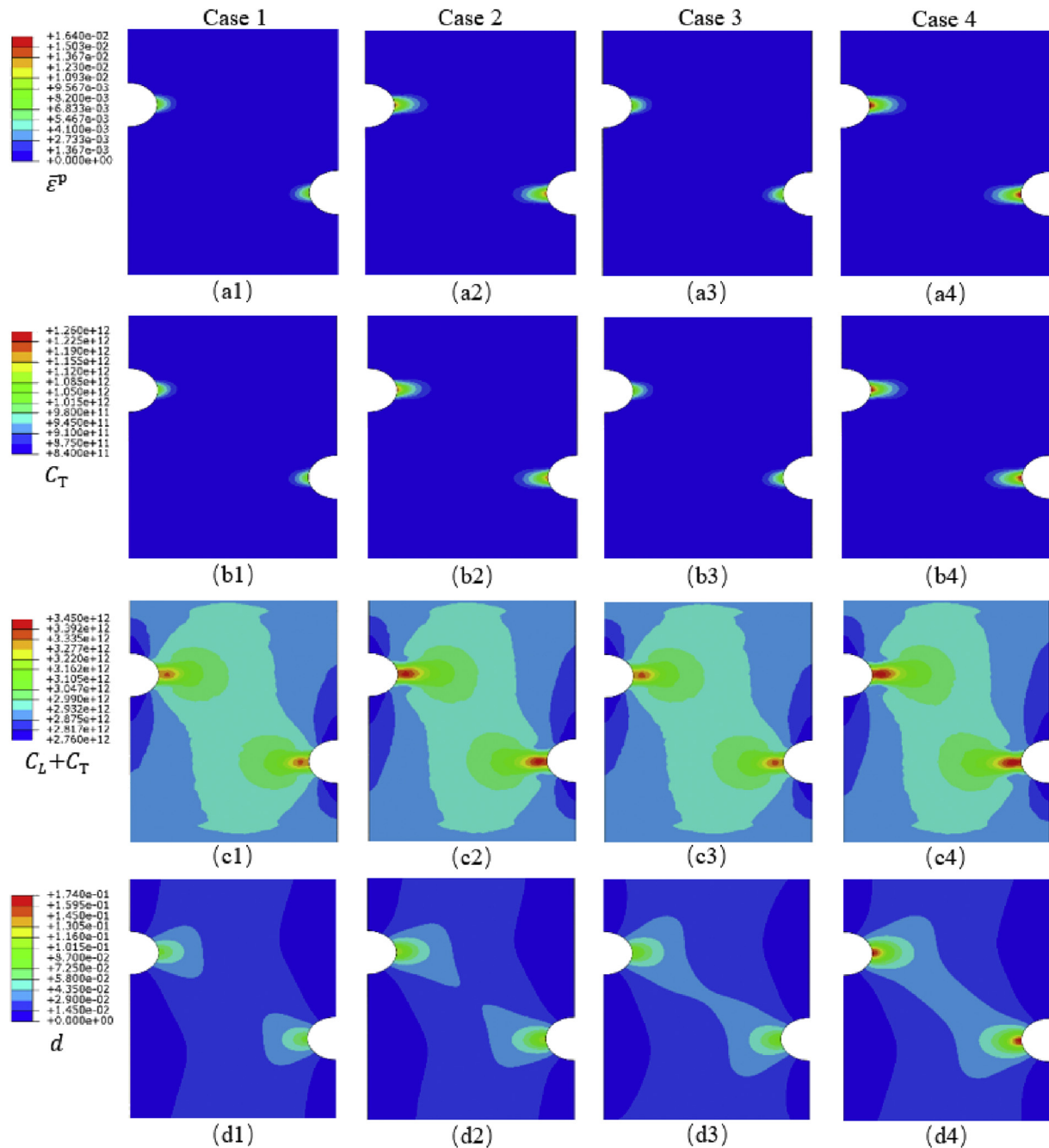
the notch tip. But comparing to Fig. 13(a1,a2,b1,b2), the effect of HEDE on plastic straining and hydrogen trapping is not as significant as the effect of HELP. Thus, the difference of the total hydrogen concentration in Fig. 14(c1,c2) is hardly noticeable. However, as a result of the reduction of the critical energy release rate caused by the HEDE effect, the crack initiation speed is still faster than the baseline case, Fig. 14(d1,d2).

Results in Figs. 13 and 14 suggest that the HELP mechanism embrittles the material by promoting local plastic deformation, and it has a strong effect on the hydrogen distribution at the notch tip. On the other hand, the HEDE mechanism does not show a strong influence on the hydrogen redistribution prior to crack initiation, but it embrittles the material by reducing the critical energy release rate.

Fig. 15 examines how HELP and HEDE mechanisms work together by comparing the simulation results of 4 cases at the loading stage 3 indicated in Fig. 12. Both HELP (a2, b2, c2, d2) and HEDE (a3, b3, c3, d3) facilitate plastic straining and

Fig. 15 – Distributions of the effective plastic strain (a1–a4), the trapped hydrogen (b1–b4), the total hydrogen (c1–c4) and the crack phase field value (d1–d4) on the mid-surface of the specimen for case 1 (a1, b1, c1, d1), case 2 (a2, b2, c2, d2), case 3 (a3, b3, c3, d3) and case 4 (a4, b4, c4, d4), at the loading stage 3 indicated in Fig. 12.

promote hydrogen trapping at the notch tip. But the effect of HEDE is not as significant as the effect of HELP. Thus, the difference of the total hydrogen concentration in c1 and c3 is hardly noticeable. It is worth noting that neither HELP nor HEDE alone significantly promotes crack initiation at loading stage 3 (d1, d2, d3). When HELP and HEDE mechanisms work together, leading to more plastic straining and hydrogen trapping at the notch tip (a4, b4), the total hydrogen concentration is close to the result when only HELP mechanism is concerned (c2, c4). As a result of the combination of HELP and

HEDE mechanisms, the crack initiation speed is faster than the cases with only one mechanism is considered (d2, d3, d4).

The above results indicate that the mechanisms of HELP and HEDE, when considered separately, each can promote crack initiation and lead to material embrittlement. When both mechanisms are considered, the combined effect on hydrogen embrittlement is more significant than when only one mechanism is considered. HELP reduces the local yield stress and HEDE reduces the critical energy release rate, and the two mechanisms work concurrently after plastic

deformation develops. The correlation of both mechanisms is through the material response influenced by them.

Conclusions

This study presents a numerical model for hydrogen embrittlement at the macroscopic scale. A previously proposed phase field method is extended by incorporating hydrogen transport and the resulting HELP and HEDE effects into the governing equations. The equation controlling hydrogen diffusion through lattice sites is modified to include the effect of the crack phase field. A new trapping density function is proposed so that the trapped hydrogen remains on the newly created crack surfaces but the concentration does not increase during crack propagation. The HELP effect is modeled by reducing the yield stress with the presence of hydrogen and the HEDE effect is modeled by reducing the critical energy release rate with hydrogen concentration. A compact tension specimen and a flat specimen with a double notch are used to demonstrate the numerical model. Results of a series of numerical simulations suggest that:

- Hydrogen atoms tend to accumulate at the crack/notch tip region since the positive hydrostatic stress in this area promotes lattice hydrogen cumulation and the plastic deformation in this area generates more traps.
- HELP promotes the localization of plastic strain and accelerates material failure. The load carrying capacity of the specimen decreases as the value of the HELP parameter ϑ decreases.
- HEDE reduces the critical energy release rate and facilitates crack propagation. The load carrying capacity of the specimen decreases as the value of the HEDE parameter ζ decreases.
- The proposed numerical model, which combines the HELP and HEDE effects, can comprehensively simulate hydrogen embrittlement and predict the transition from ductile to brittle caused by the presence of hydrogen.

R E F E R E N C E S

[1] Johnson WH. On some remarkable changes produced in iron and steel by the action of hydrogen and acids. Nature 1875;11:393. https://doi.org/10.1038/011393a0.

[2] Robertson IM, Sofronis P, Nagao A, Martin ML, Wang S, Gross DW, et al. Hydrogen embrittlement understood. Metall Mater Trans Phys Metall Mater Sci 2015;46:2323–41. https://doi.org/10.1007/s11661-015-2836-1.

[3] Oriani R. The diffusion and trapping of hydrogen in steel. Acta Metall 1970;18:147–57. https://doi.org/10.1016/0001-6160(70)90078-7.

[4] Sofronis P, McMeeking RM. Numerical analysis of hydrogen transport near a blunting crack tip. J Mech Phys Solid 1989;37:317–50. https://doi.org/10.1016/0022-5096(89)90002-1.

[5] Kumnick AJ, Johnson HH. Deep trapping states for hydrogen in deformed iron. Acta Metall 1980;28:33–9. https://doi.org/10.1016/0001-6160(80)90038-3.

[6] Lufrano J, Sofronis P. Enhanced hydrogen concentrations ahead of rounded notches and cracks-competition between plastic strain and hydrostatic stress. Acta Mater 1998;46:1519–26. https://doi.org/10.1016/S1359-6454(97)00364-9.

[7] Oriani RA. A mechanistic theory of hydrogen embrittlement of steels. Ber Bunsen Ges Phys Chem 1972;76:848–57. https://doi.org/10.1002/BBPC.19720760864.

[8] Oriani RA. Hydrogen - the versatile embrittler. Corrosion 1987;43:390–7. https://doi.org/10.5006/1.3583875.

[9] Dwivedi SK, Vishwakarma M. Hydrogen embrittlement in different materials: a review. Int J Hydrogen Energy 2018;43:21603–16. https://doi.org/10.1016/j.ijhydene.2018.09.201.

[10] Beachem CD. A new model for hydrogen-assisted cracking (hydrogen "embrittlement"). Metall Mater Trans 1972;3:441–55. https://doi.org/10.1007/BF02642048.

[11] Robertson IM, Birnbaum HK. An HVEM study of hydrogen effects on the deformation and fracture of nickel. Acta Metall 1986;34:353–66. https://doi.org/10.1016/0001-6160(86)90071-4.

[12] Birnbaum HK, Sofronis P. Hydrogen-enhanced localized plasticity-a mechanism for hydrogen-related fracture. Mater Sci Eng, A 1994;176:191–202. https://doi.org/10.1016/0921-5093(94)90975-X.

[13] Ferreira PJ, Robertson IM, Birnbaum HK. Hydrogen effects on the interaction between dislocations. Acta Mater 1998;46:1749–57. https://doi.org/10.1016/S1359-6454(97)00349-2.

[14] Sofronis P, Robertson IM. Transmission electron microscopy observations and micromechanical/continuum models for the effect of hydrogen on the mechanical behaviour of metals. Philos Mag A 2002;82:3405–13. https://doi.org/10.1080/01418610208240451.

[15] Matsui H, Kimura H, Moriya S. The effect of hydrogen on the mechanical properties of high purity iron I. Softening and hardening of high purity iron by hydrogen charging during tensile deformation. Mater Sci Eng 1979;40:207–16. https://doi.org/10.1016/0025-5416(79)90191-5.

[16] Moriya S, Matsui H, Kimura H. The effect of hydrogen on the mechanical properties of high purity iron II. Effect of quenched-in hydrogen below room temperature. Mater Sci Eng 1979;40:217–25. https://doi.org/10.1016/0025-5416(79)90192-7.

[17] Ferreira PJ, Robertson IM, Birnbaum HK. Hydrogen effects on the interaction between dislocations. Acta Mater 1998;46:1749–57. https://doi.org/10.1016/S1359-6454(97)00349-2.

[18] Robertson IM. The effect of hydrogen on dislocation dynamics. Eng Fract Mech 1999;64:649–73. https://doi.org/10.1016/S0013-7944(99)00094-6.

[19] Birnbaum HK, Sofronis P. Hydrogen-enhanced localized plasticity-a mechanism for hydrogen-related fracture. Mater Sci Eng, A 1994;176:191–202. https://doi.org/10.1016/0921-5093(94)90975-X.

[20] Liang Y, Ahn DC, Sofronis P, Dodds RH, Bammann D. Effect of hydrogen trapping on void growth and coalescence in metals and alloys. Mech Mater 2008;40:115–32. https://doi.org/10.1016/j.mechmat.2007.07.001.

[21] Huang C, Luo T, Gao X, Graham SM. Modeling the effect of hydrogen on ductile fracture. Mater Perform Char 2018;7:101–18. https://doi.org/10.1520/mpc20170073.

[22] Luo T, Huang C, Gao X. An investigation of the effect of hydrogen on ductile fracture using a unit cell model. Int J Hydrogen Energy 2019;44(16):8627–40. https://doi.org/10.1016/j.ijhydene.2019.02.069.

[23] Yu H, Olsen JS, He J, Zhang Z. Hydrogen-microvoid interactions at continuum scale. Int J Hydrogen Energy 2018;43:10104–28. https://doi.org/10.1016/j.ijhydene.2018.04.064.

[24] Depover T, Verbeken K. The detrimental effect of hydrogen at dislocations on the hydrogen embrittlement susceptibility

of Fe-C-X alloys: an experimental proof of the HELP mechanism. Int J Hydrogen Energy 2018;43:3050—61. https://doi.org/10.1016/j.ijhydene.2017.12.109.

[25] Petch NJ, Stables P. Delayed fracture of metals under static load. Nature 1952;169:842—3. https://doi.org/10.1038/169842a0.

[26] Petch NJ. The lowering of fracture-stress due to surface adsorption. Philos Mag A 1956;1:331—7. https://doi.org/10.1080/14786435608238106.

[27] Tromans D. On surface energy and the hydrogen embrittlement of iron and steels. Acta Metall Mater 1994;42:2043—9. https://doi.org/10.1016/0956-7151(94)90029-9.

[28] Depover T, Wallaert E, Verbeken K. Fractographic analysis of the role of hydrogen diffusion on the hydrogen embrittlement susceptibility of DP steel. Mater Sci Eng, A 2016;649:201—8. https://doi.org/10.1016/j.msea.2015.09.124.

[29] Troiano RA. The role of hydrogen and other interstitials in the mechanical behavior of metals. Trans ASM 1960;52:54—80.

[30] Jiang DE, Carter EA. First principles assessment of ideal fracture energies of materials with mobile impurities: implications for hydrogen embrittlement of metals. Acta Mater 2004;52:4801—7. https://doi.org/10.1016/J.ACTAMAT.2004.06.037.

[31] Serebrinsky S, Carter EA, Ortiz M. A quantum-mechanically informed continuum model of hydrogen embrittlement. J Mech Phys Solid 2004;52:2403—30. https://doi.org/10.1016/J.JMPS.2004.02.010.

[32] Martínez-Pañeda E, Golahmar A, Niordson CF. A phase field formulation for hydrogen assisted cracking. Comput Methods Appl Mech Eng 2018;342:742—61. https://doi.org/10.1016/j.cma.2018.07.021.

[33] Wang S, Martin ML, Robertson IM, Sofronis P. Effect of hydrogen environment on the separation of Fe grain boundaries. Acta Mater 2016;107:279—88. https://doi.org/10.1016/j.actamat.2016.01.067.

[34] Griffith AA. The phenomena of rupture and flow in solids. Philos Trans R Soc Lond A Math Phys Sci 1921;221:163—98. https://doi.org/10.1098/rsta.1921.0006.

[35] Francfort GA, Marigo JJ. Revisiting brittle fracture as an energy minimization problem. J Mech Phys Solid 1998;46:1319—42. https://doi.org/10.1016/S0022-5096(98)00034-9.

[36] Bourdin B, Francfort GA, Marigo JJ. Numerical experiments in revisited brittle fracture. J Mech Phys Solid 2000;48:797—826. https://doi.org/10.1016/S0022-5096(99)00028-9.

[37] Bourdin B, Francfort GA, Marigo J-J. The variational approach to fracture. J Elasticity 2008;91:5—148. https://doi.org/10.1007/s10659-007-9107-3.

[38] Miehe C, Welschinger F, Hofacker M. Thermodynamically consistent phase-field models of fracture: variational principles and multi-field FE implementations. Int J Numer Methods Eng 2010;83:1273—311. https://doi.org/10.1002/nme.2861.

[39] Miehe C, Hofacker M, Welschinger F. A phase field model for rate-independent crack propagation: robust algorithmic implementation based on operator splits. Comput Methods Appl Mech Eng 2010;199:2765—78. https://doi.org/10.1016/j.cma.2010.04.011.

[40] Miehe C, Hofacker M, Schänzel LM, Aldakheel F. Phase field modeling of fracture in multi-physics problems. Part II. Coupled brittle-to-ductile failure criteria and crack propagation in thermo-elastic-plastic solids. Comput Methods Appl Mech Eng 2015;294:486—522. https://doi.org/10.1016/j.cma.2014.11.017.

[41] Ambati M, Gerasimov T, De Lorenzis L. Phase-field modeling of ductile fracture. Comput Mech 2015;55:1017—40. https://doi.org/10.1007/s00466-015-1151-4.

[42] Ambati M, Kruse R, De Lorenzis L. A phase-field model for ductile fracture at finite strains and its experimental verification. Comput Mech 2016;57:149—67. https://doi.org/10.1007/s00466-015-1225-3.

[43] Borden MJ, Hughes TJR, Landis CM, Anvari A, Lee IJ. A phase-field formulation for fracture in ductile materials: finite deformation balance law derivation, plastic degradation, and stress triaxiality effects. Comput Methods Appl Mech Eng 2016;312:130—66. https://doi.org/10.1016/j.cma.2016.09.005.

[44] Huang C, Gao X. Development of a phase field method for modeling brittle and ductile fracture. Comput Mater Sci 2019;169:109089. https://doi.org/10.1016/J.COMMATSCI.2019.109089.

[45] Krom AHM. Numerical modelling of hydrogen transport in steel. 1998.

[46] Kumnick AJ, Johnson HH. Deep trapping states for hydrogen in deformed iron. Acta Metall 1980;28:33—9. https://doi.org/10.1016/0001-6160(80)90038-3.

[47] Taha A, Sofronis P. A micromechanics approach to the study of hydrogen transport and embrittlement. Eng Fract Mech 2001;68:803—37. https://doi.org/10.1016/S0013-7944(00)00126-0.

[48] Song J, Curtin WA. Atomic mechanism and prediction of hydrogen embrittlement in iron. Nat Mater 2013;12:145—51. https://doi.org/10.1038/nmat3479.

[49] Sofronis P, Liang Y, Aravas N. Hydrogen induced shear localization of the plastic flow in metals and alloys. Eur J Mech Solid 2001;20:857—72. https://doi.org/10.1016/S0997-7538(01)01179-2.

[50] Liang Y, Sofronis P, Aravas N. On the effect of hydrogen on plastic instabilities in metals. Acta Mater 2003;51:2717—30. https://doi.org/10.1016/S1359-6454(03)00081-8.

[51] Oriani RA, Josephic PH. Equilibrium aspects of hydrogen-induced cracking of steels. Acta Metall 1974;22:1065—74. https://doi.org/10.1016/0001-6160(74)90061-3.

[52] Frohmberg RP, Barnett WJ, Troiano AR. Delayed failure and hydrogen embrittlement in steel. WADC Technical Report 54-320. 1954.

[53] Johnson H, Army F. Hydrogen , crack initiation , and delayed failure in steel. OstiGov 1956;3.